Dynamic Model and Instability Evaluation of an Articulated Mobile Agri-Robot

G. Carabin, R. Vidoni, F. Mazzetto and A. Gasparetto

Abstract Stability, in particular in outdoor sloped conditions, is one of the most important requirements for design safe and effective future mobile robotic platforms. In this work, the authors' recent results on the study and development of an articulated mobile robot for agricultural and forestry activities in hilly/mountain environments are presented. First of all, a dynamic model for the stability analysis of a generic articulated platform has been designed and implemented. Then, different practical working conditions have been simulated to assess the stability of the system; possible stabilizing actions when travelling on a sloped surface on the steering angle, velocity and central joint have been finally evaluated and discussed.

Keywords Articulated joint · Mobile robot · Stability · Agricultural robotics

1 Introduction

Among different possible mobile robot architectures, the 4-wheeled articulated kinematics is one of the most promising [1]. Basically, it is composed of two main parts, i.e. front (f) and rear (r), interconnected by an articulated 2 Degrees of Freedom (DoF) joint. The first DoF, i.e. yaw angle, is controlled and allows steering. The second DoF is passive, i.e. roll angle, allowing to adapt to uneven terrains.

G. Carabin · R. Vidoni (✉) · F. Mazzetto
FaST (Faculty of Science and Technology), Free University of Bolzano,
39100 Bolzano, Italy
e-mail: renato.vidoni@unibz.it

G. Carabin
e-mail: giovanni.carabin@unibz.it

F. Mazzetto
e-mail: fabrizio.mazzetto@unibz.it

A. Gasparetto
DPIA (Dipartimento Politecnico di Ingegneria e Architettura), University of Udine,
33100 Udine, Italy
e-mail: gasparetto@uniud.it

G. Boschetti and A. Gasparetto (eds.), *Advances in Italian Mechanism Science*,
Mechanisms and Machine Science 47, DOI 10.1007/978-3-319-48375-7_36

With this architecture a minimal steering radius, if compared with other classical kinematics, is achievable. In literature, monitoring and predicting the stability of a mobile platform is a well treated problem. Indeed, the stability of multi-legged or -wheeled robots has been widely investigated since the sixties, e.g. [2], in particular for rigid chassis machines. Two main classes of stability criteria have been proposed: (quasi-)static and dynamics-based criteria. These can also be grouped in: *distance-based* [2], *angle-based* [3], *energy-based* [4], *moment-based* [5] and *force-based* criteria [6], according to the idea behind the formulation. Recent stability studies on articulated architectures refer to tractors/machines with the joint on the front axle [7, 8] demonstrated how, in addition to the "standard" stability condition (type II instability), the passive roll DoF creates a second critical stability condition that results in the triangle which is made by considering the position of two wheels of a vehicle half and the joint (type I instability).

2 Articulated Mobile Robot Model

The kinematic and dynamic model is based on the main basic hypothesis of the Guzzomi's work [7] except for the robot speed. These are: (a) the roll DoF of the articulated joint is considered frictionless; (b) the robot does not slide down the slope, due to a non-limiting coefficient of friction between surface and tyres; (c) tyres are considered stiff, so the contact surfaces result in discrete points (not areas); (d) the joint mass is negligible, so it does not affect the dynamic behaviour.

By referring at Fig. 1a, the articulated robot kinematics can be explained. The front "f" and rear "r" parts are connected by a 2 DoF joint made of a first revolute DoF, i.e. the yaw β angle, and a second passive revolute DoF, i.e. the roll α angle. In Table 1, the geometric parameters of the model shown in Fig. 1a are explained.

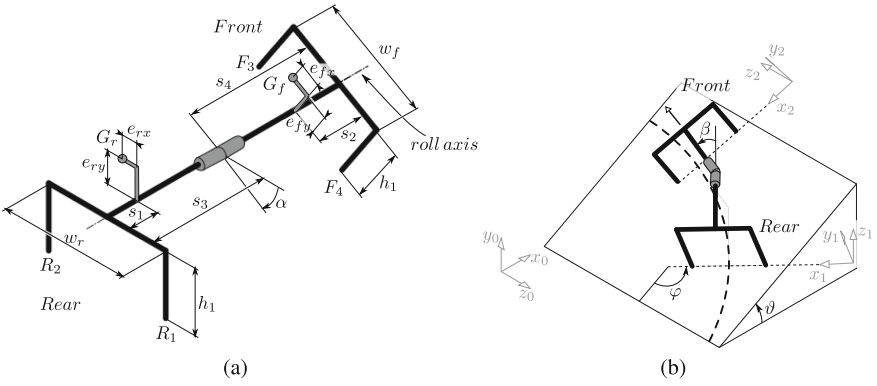

Fig. 1 Articulated robot: **a** kinematic model ($\alpha \neq 0$ and $\beta = 0$), **b** orientation angles and reference systems ($\alpha = 0$ and $\beta \neq 0$)

Table 1 Main parameters of the kinematic model

G_r	CoG of the rear part	s_4	Distance from front axle to central joint
G_f	CoG of the front part	s_1	Rear CoG distance from rear axle
R_1	Contact point between rear wheel 1 and surface	e_{rx}	Rear CoG x distance from rear midplane
		e_{ry}	Rear CoG y height above roll axis
R_2	Contact point between rear wheel 2 and surface	s_2	Front CoG distance from front axle
		e_{fx}	Front CoG x distance from front midplane
F_3	Contact point between front wheel 3 and surface	e_{fy}	Front CoG y height above roll axis
		w_r	Rear track width
F_4	Contact point between front wheel 4 and surface	w_f	Front track width
		h_1	Roll axis height from ground
α	Roll angle between rear and front part	m_r	Rear mass
β	Yaw angle between rear and front part	m_f	Front mass
s_3	Distance from rear axle to central joint		

In order to study the system configurations, both travelling along a slope and turning among different rows, the robot has been considered travelling a circle with a constant speed v on a sloped surface, i.e. ϑ. A global coordinate system $(x_0\, y_0\, z_0)$ and two local ones $(x_1\, y_1\, z_1)$ and $(x_2\, y_2\, z_2)$, rigidly attached on the moving rear and front robot parts respectively, are defined. By naming φ the robot orientation with respect to the maximum slope direction, β the trajectory followed by the robot and α the surface conformation ($\alpha = 0$ implies a plane surface), see Fig. 1b, the kinematics of the motion can be represented.

2.1 Dynamic Model

The instability of an articulated robot can be subdivided in phase I and II [7]. By increasing the slope, the force distribution on the four wheels changes according to the configuration and system properties. Instability occurs when one of the four reaction forces falls to zero. After that, the roll moment equilibrium is not satisfied, one wheel loses the contact and the phase I instability occurs.

As drawn in Fig. 2a, b, two $\mathbf{F_{Gr}}$ and $\mathbf{F_{Gf}}$ forces are present on the rear and front CoGs, given by the vectorial sum between weight $\mathbf{P_i}$ and centrifugal $\mathbf{F_{ci}}$ forces. These are counteracted by the four reaction forces $\mathbf{F_{r1}}$, $\mathbf{F_{r2}}$, $\mathbf{F_{f3}}$ and $\mathbf{F_{f4}}$. Through the central joint, both forces ($\mathbf{F_{jr}}$ and $\mathbf{F_{jf}}$) and moments ($\mathbf{M_r}$ e $\mathbf{M_f}$) are exchanged. The two forces $\mathbf{F_{Gr}}$ and $\mathbf{F_{Gf}}$ and, due to the absence of friction, the moment $M_{f,z}$ are known.

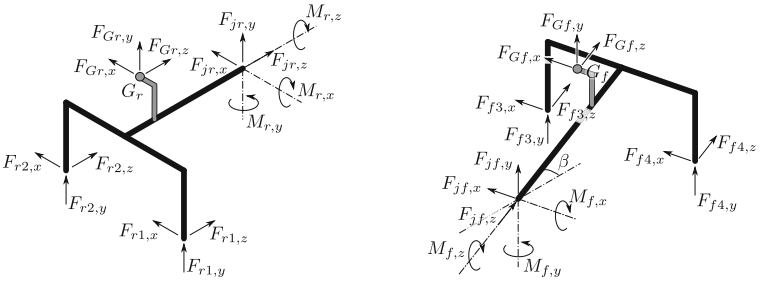

Fig. 2 Dynamic model: **a** rear part, **b** front part

To study the stability, the four normal force components acting on the wheels, i.e. $F_{r1,y}$, $F_{r2,y}$, $F_{f3,y}$ and $F_{f4,y}$, are needed. Thus, it is advisable to reduce the system dimension to improve the computational speed with respect to solve the whole system made of 23 equations. By exploiting the joint forces and torques relationships as well as the ones between the exchanged forces on the wheels and those acting on the CoGs, the problem can be reformulated and simplified from the initial 23 to 6 unknowns: F_{r1}, F_{r2}, F_{f3}, F_{f4}, $M_{f,x}$ and $M_{f,y}$. In such a manner, six equilibrium equations in 6 unknowns (F_{r1}, F_{r2}, F_{f3}, F_{f4}, $M_{f,x}$ and $M_{f,y}$) can be written:

$$F_{r1} + F_{r2} + F_{f3} + F_{f4} = -F_{Gr} - F_{Gf} \tag{1}$$

$$M_{f,x} + F_{f3}\left(-k_{fy}s_4 - k_{fz}h_1\right) + F_{f4}\left(-k_{fy}s_4 - k_{fz}h_1\right) = F_{gf}\left[k_{fy}\left(s_4 - s_2\right) + k_{fz}e_{fy}\right] \tag{2}$$

$$M_{f,y} + F_{f3}\left(k_{fx}s_4 - k_{fz}\frac{w_f}{2}\right) + F_{f4}\left(k_{fx}s_4 + k_{fz}\frac{w_f}{2}\right) = F_{gf}\left[-k_{fx}\left(s_4 - s_2\right) + k_{fz}e_{fx}\right] \tag{3}$$

$$M_{f,z} + F_{f3}\left(k_{fx}h_1 + k_{fy}\frac{w_f}{2}\right) + F_{f4}\left(k_{fx}h_1 - k_{fy}\frac{w_f}{2}\right) = F_{gf}\left(k_{fx}e_{fy} - k_{fy}e_{fx}\right) \tag{4}$$

$$M_{r,x} + F_{r1}\left(k_{ry}s_3 - k_{rz}h_1\right) + F_{r2}\left(k_{ry}s_3 - k_{rz}h_1\right) = F_{gr}\left[-k_{ry}\left(s_3 - s_1\right) - k_{rz}e_{ry}\right] \tag{5}$$

$$M_{r,z} + F_{r1}\left(k_{rx}h_1 - k_{ry}\frac{w_r}{2}\right) + F_{r2}\left(k_{rx}h_1 + k_{ry}\frac{w_r}{2}\right) = F_{gr}\left(k_{rx}e_{ry} - k_{ry}e_{rx}\right) \tag{6}$$

where $M_{f,z} = 0$, $M_{r,x} = -M_{f,x}\cos\alpha\cos\beta + M_{f,y}\sin\alpha\cos\beta$, $M_{r,z} = M_{f,x}\cos\alpha\sin\beta - M_{f,y}\sin\alpha\sin\beta$, $\left(k_{rx}, k_{ry}, k_{rz}\right) = \frac{\mathbf{F_{Gr}}}{\|\mathbf{F_{Gr}}\|}$, and $\left(k_{fx}, k_{fy}, k_{fz}\right) = \frac{\mathbf{F_{Gf}}}{\|\mathbf{F_{Gf}}\|}$.

The rear and front weight forces components can then be computed. Moreover, the rear and front centrifugal forces components while, see Fig. 3a, are:

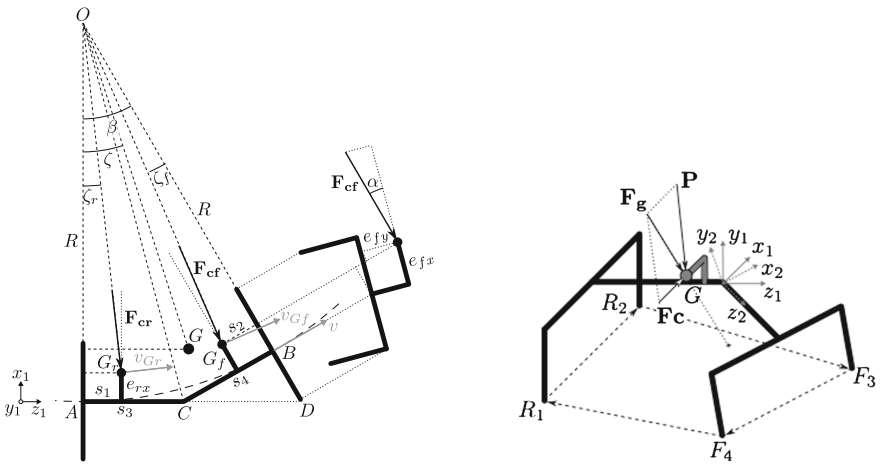

Fig. 3 **a** Centrifugal forces. **b** Phase II instability

$$\begin{Bmatrix} F_{cr,x} \\ F_{cr,y} \\ F_{cr,z} \end{Bmatrix} = F_{cr} \begin{Bmatrix} -\cos\zeta_r \\ 0 \\ \sin\zeta_r \end{Bmatrix} \qquad \begin{Bmatrix} F_{cf,x} \\ F_{cf,y} \\ F_{cf,z} \end{Bmatrix} = F_{cf} \begin{Bmatrix} -\cos\zeta_f \cos\alpha \\ \sin\alpha \\ -\sin\zeta_f \cos\alpha \end{Bmatrix} \tag{7}$$

where ζ_r and ζ_f angles are computed as:

$$\zeta_r = \arctan\left(\frac{s_1}{R - e_{rx}}\right) \qquad \zeta_f = \arctan\left(\frac{s_2}{R - e_{fx}\cos\alpha + e_{fy}\sin\alpha}\right) \tag{8}$$

Given a β angle, it is possible to compute the steering radius R in the following manner (see Fig. 3a):

$$R = \frac{\overline{AD}}{\tan\beta} = \frac{\overline{AC} + \frac{\overline{BC}}{\cos\beta}}{\tan\beta} = \frac{s_3\cos\beta + s_4}{\sin\beta} \tag{9}$$

Now, by considering as reference the rear/front axle central point speed v, the CoGs speeds v_{Gr} and v_{Gr} and the centrifugal forces can be computed (see Fig. 3):

$$v_{Gi} = v\frac{R_{Gi}}{R} \qquad R_{Gi} = \frac{s_j}{\sin\zeta_i} \qquad F_{ci} = \frac{m_i v_{Gi}^2}{R_{Gi}} = \frac{m_i v^2 R_{Gi}}{R^2} \tag{10}$$

with i = r, f and j = 1, 2. The vectorial sum between weight and centrifugal forces allows then to compute the two forces F_{Gr} and F_{Gf}.

The phase II instability detection method is based on force moments evaluation. The dashed lines in Fig. 3b represent the four oriented axes that pass through the four contact points. The robot could rotate around these axes, if there is no moment equilibrium. The force $\mathbf{F_g}$, that acts on the overall Center of Gravity G, generates four different moments on every axis. So, in a given robot configuration, if all the moments are positive, there is stability; if one of the moments becomes negative, the robot starts overturning. The global CoG coordinates can be obtained starting from G_r and G_f and, then, the force $\mathbf{F_g}$, expressed with respect to the $\left(x_1\, y_1\, z_1\right)$ reference system, can be computed as $\mathbf{F_g} = \mathbf{P} + \mathbf{F_c}$, where $P = \left(m_r + m_f\right) g$, and $F_c = \frac{\left(m_r+m_f\right)v^2 R_G}{R^2}$ with $R_G = \frac{G_z}{\sin\zeta}$ (see Fig. 3a).

3 Numerical Evaluation

The stability model has been implemented in a Matlab™ simulator. Given information on the geometric and physical parameters of the robot (see Table 2), and on the configuration in terms of α, β and φ angles, via an iterative method the stability limit angles of phase I, i.e. $\vartheta_{lim,I}$, and phase II, i.e. $\vartheta_{lim,II}$, are found. In Fig. 4, the output of the simulator is reported: the top plot refers to the limit stability angles while the central plot indicates which wheel firstly detaches from the terrain when phase I instability occurs; finally, the plot on the bottom reports the angular difference between phase II and phase I critical angles.

Now, the centrifugal terms influence on the emulator stability is evaluated. A constant steering angle, i.e. $\beta = 15°$, and three different speeds ($v = 0\ ^{\mathrm{m}}/_{\mathrm{s}}$, $v = 0.75\ ^{\mathrm{m}}/_{\mathrm{s}}$ and $v = 1.5\ ^{\mathrm{m}}/_{\mathrm{s}}$) are considered. In Fig. 4, the curve with no centrifugal influence, i.e. $v = 0\ ^{\mathrm{m}}/_{\mathrm{s}}$ quasi-static approach, and the others are reported.

In the simulated case it can be easily highlighted how the centrifugal force plays against stability, both in phase I and II, when φ is inside the range of about $-80°(280°) \div 80°$ (i.e. centrifugal forces are directed downstream). Furthermore this range tends to become larger if the speed increases. Varying the robot speed could represent a driving strategy, or a part of it, combined with a blocking action on the joint free DoF; indeed, in that manner, a safer stability state could be reached while maintaining the same configuration. Considering the range where the centrifugal effect plays against the stability, decreasing the speed helps increasing the stability. This strategy, if $v > 0.75\ ^{\mathrm{m}}/_{\mathrm{s}}$, guarantees a higher angular margin with respect to blocking the joint. Below that speed the two effects are comparable. Outside this

Table 2 Robot emulator geometric and physical parameters

s_1 [mm]	s_2 [mm]	s_3 [mm]	s_4 [mm]	w_r [mm]	w_f [mm]	h_1 [mm]	e_{rx} [mm]	e_{fx} [mm]	e_{ry} [mm]	e_{fy} [mm]	m_r [kg]	m_f [kg]
26	55	200	200	240	180	94	0	0	20	14	1.34	1.84

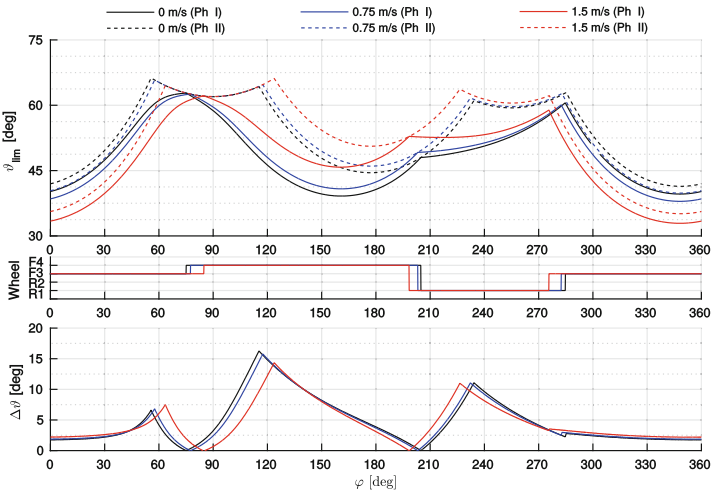

Fig. 4 Stability maps at different speeds ($\beta = 15°$)

range, decreasing the speed becomes a dangerous manoeuvre. Considering $\varphi \simeq 0$, i.e. the robot on the lower point of the circular trajectory, the centrifugal effect is maximum. In this condition, it is interesting to evaluate this stability angle reduction. At speed $v = 0\ ^{m}/_{s}$, the phase I stability angle is about 40°, at $v = 0.75\ ^{m}/_{s}$ the reduction is about 2°, and at $v = 1.5\ ^{m}/_{s}$ it is about 7°. For the phase II case, the values are almost the same. Now, if the angular margin that is gained by blocking the free joint DoF (see the bottom plot of Fig. 4), it could be seen that the centrifugal forces affect only the curves offset.

The transition between different sloped surfaces is another important case to be evaluated. In order to do so, the following condition has been considered:

- the base surface is inclined by an angle of $\vartheta = 15°$;
- the robot runs crosswise the slope ($\varphi = 0°$);
- on the base surface it is located another plane (obstacle) that gradually increases its inclination from ϑ to $\vartheta + \alpha$;
- this obstacle is overcome firstly by the front part, and then by the rear one.

In Fig. 5 the results are presented. Firstly considering the front part overcoming the obstacle, by increasing α, i.e. higher obstacle inclination, the angular margin for the roll-over decreases. However, the phase I and phase II have different negative slopes (less in the second case), so it is possible to gain stability margin by blocking the free DoF. It can be noticed how the instability concerns only the front part, but with the base inclination considered, $\vartheta = 15°$, the roll-over does not occur (i.e. the $\vartheta_{lim} - \vartheta$ values reported in the figure is always positive). When the rear part overcomes the obstacle, two different phase I instability behaviours can be observed. Until $\alpha < 8°$, the angle at which instability occurs remains constant; indeed, in this configuration, the front part is the one more critical and it is not influenced by an α

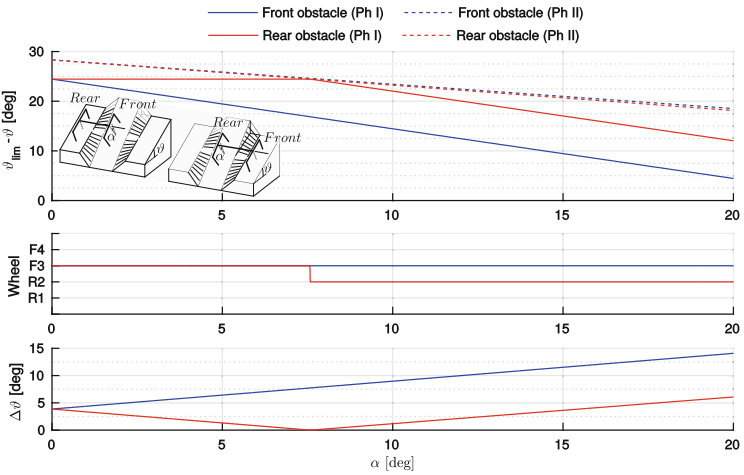

Fig. 5 Front and rear parts passing the obstacle (15° of plane inclination)

variation. When $\alpha > 8°$, the rear part becomes the most critical in terms of phase I stability and the angular margin decreases with α. Also in this case the phase II has a negative constant slope, thus the support polygon reduces its area and the stability margin is reduced.

4 Conclusion

In this paper, an articulated kinematics has been chosen as basis of a future mobile robot able to operate in hilly terrains. After the definition of the dynamic model, the two main instabilities of the chosen platform has been discussed and a stability criterion chosen. The implemented model have been exploited for evaluating the critical configurations on different slopes; after that, given the importance of the working speed and of the current slope, the possible stabilizing effect of speed and steering angle variation, together with a blocking of the joint passive DoF have been simulated and highlighted.

References

1. Vidoni R, Bietresato M, Gasparetto A, Mazzetto F (2015) Evaluation and stability comparison of different vehicle configurations for robotic agricultural operations on side-slopes. Biosyst Eng 129:197–211
2. McGhee R, Frank A (1968) On the stability properties of quadruped creeping gaits. Math. Biosci. 3:331–351

3. Papadopoulos E, Rey D (2000) The force-angle measure of tipover stability margin for mobile manipulators. Veh Syst Dyn 33:29–48
4. Davidson JK, Schweitzer G (1990) A mechanics-based computer algorithm for displaying the margin of static stability in four-legged vehicles. Trans ASME J Mech Des 112:480–487
5. Lee J, Park J, Lee B (2009) Turnover prevention of a mobile robot on uneven terrain using concept of stability space. Robotica 27:641–652
6. Agheli M, Nestinger S (2012) Study of the foot force stability margin for multi-legged/wheeled robots under dynamic situations. In: 2012 IEEE/ASME International Conference on Mechatronics and embedded systems and applications (MESA), pp 99–104, July 2012
7. Baker V, Guzzomi AL (2013) A model and comparison of 4-wheel-drive fixed-chassis tractor rollover during phase I. Biosyst Eng 116(2):179–189
8. Li Z, Mitsuokab M, Inoueb E, Okayasub T, Hiraib Y (2015) Development of stability indicators for dynamic phase I overturn of conventional farm tractors with front axle pivot. Biosyst Eng 134:55–57